Experimental Stability Study of Modulated Model Predictive Current Controllers Applied to Six-Phase Induction Motor Drives

Magno Ayala, Jesus Doval-Gandoy, *Member, IEEE*, Osvaldo Gonzalez, Jorge Rodas, Raul Gregor, and Marco Rivera, *Senior Member, IEEE*

***Abstract*—Modulated model predictive current control techniques are considered an interesting option to control multiphase drives due to their control flexibility and fast dynamic response. However, a practical stability study of those techniques is still missing. This article presents an experimental stability study, to quantify the limits of stability, to modulated predictive current controllers applied to an asymmetrical six-phase induction machine. Experimental results are presented to verify the theoretical analysis results in terms of stability ranges regarding sampling frequency and rotor speed.**

***Index Terms*—Multiphase induction machine, model predictive control (MPC), practical stability, space vector modulation.**

I. Introduction

MODULATED model predictive current controllers have gained attention in the last years as valid alternatives to conventional model predictive current control (MPCC) techniques [1]–[4] as MPCC has shown very good results in comparison to linear PI controllers, in terms of faster transient dynamics, easier inclusions of constraints, among others, applied in electrical machines [5]–[7]. At the same time, the field of multiphase induction machines (IMs) has been growing significantly in the last years [8], [9]. Comparing to the conventional three-phase IM, multiphase IMs have some intrinsic advantages such as lower torque ripple, lower current/power per phase, availability, and fault-tolerant capabilities [8], [10]–[12]. By considering these advantages, they were extensively applied in the high-power applications such as renewable energies and electric vehicles [13], [14].

As the research of multiphase IM has been growing, new nonlinear control methods were developed to apply to these machines such as sliding mode control [15], [16], fuzzy logic [17], [18], backstepping [19], [20], model referenced adaptation system [21], and new variants of modulated finite control set model predictive control (FCS-MPC) [22]–[25]. Some examples of these variants are the modulated MPC (M2PC) [26] and a novel variation named N-M2PC [27], which are considered great alternatives for low and high rotor speed operations, respectively, in terms of steady-state operations and $(x - y)$ plane (related to IM losses) currents reduction.

Furthermore, PCC stability analysis applied to different systems were approached in previous works [28], such as Buck converters and three-phase inverters [29], and synchronous machines [30]. The main common property is a defined cost function to optimize the future behavior of the system. Hence, one of the most popular methods to prove the stability of PCC is the consideration of the optimized cost function as a candidate-Lyapunov function [31]–[33]. However, this method presents many complications as to find a candidate-Lyapunov function requires complex proof. Therefore, a practical stability study of modulated PCC applied to multiphase machines in terms of sampling frequency and rotor speed has not been presented.

The main contribution of this article is an experimental stability study for M2PC and N-M2PC applied to an asymmetrical six-phase induction motor (SPIM) in terms of stability limits regarding sampling frequency and rotor speed to define the critical operating points of both techniques from the stability point of view, complementing the proposal in [27]. Experimental results are presented to verify the results of the theoretical analysis. Considering that the stability of MPCC techniques has not been analyzed in terms of sampling frequency and motor speed, it is considered that this article presents interesting results from the point of view of the design and implementation of modulated predictive control techniques. The rest of this article is organized as follows. The SPIM mathematical model is shown in Section II. In Section III, the traditional PCC design is presented and their two variants named M2PC and N-M2PC. Section IV describes the proposed theoretical stability study. Section V presents the experimental results of the system performance verifying the theoretical analysis in terms of stability ranges regarding

Manuscript received February 1, 2021; revised March 22, 2021; accepted May 13, 2021. Date of publication May 18, 2021; date of current version July 30, 2021. This work was supported in part by the CONACYT-Paraguay under Grant POSG16-05, in part by the ANID/FONDECYT/1191028 Project by SERC Chile (CONICYT/FONDAP/15110019) and in part by the Spanish State Research Agency under Project PID2019-105612RB-I00/AEI/10.13039/501100011033. Recommended for publication by Associate Editor R. Kennel. *(Corresponding author: Magno Ayala.)*

Magno Ayala, Osvaldo Gonzalez, Jorge Rodas, and Raul Gregor are with the Laboratory of Power and Control Systems, Facultad de Ingeniería, Universidad Nacional de Asunción, Luque 999999, Paraguay (e-mail: mayala@ing.una.py; ogonzalez@ing.una.py; jrodas@ing.una.py; rgregor@ing.una.py).

Jesus Doval-Gandoy is with the Applied Power Electronics Technology Research Group, Universidad de Vigo, 36310 Vigo, Spain (e-mail: jdoval@uvigo.es).

Marco Rivera is with the Department of Electrical Engineering, Universidad de Talca, Curico 3341717, Chile (e-mail: marcoriv@utalca.cl).

Color versions of one or more figures in this article are available at https://doi.org/10.1109/TPEL.2021.3081347.

Digital Object Identifier 10.1109/TPEL.2021.3081347

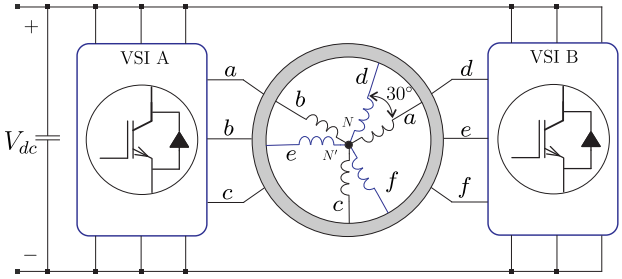

Fig. 1. Electrical scheme of a six-phase VSI connected to a SPIM.

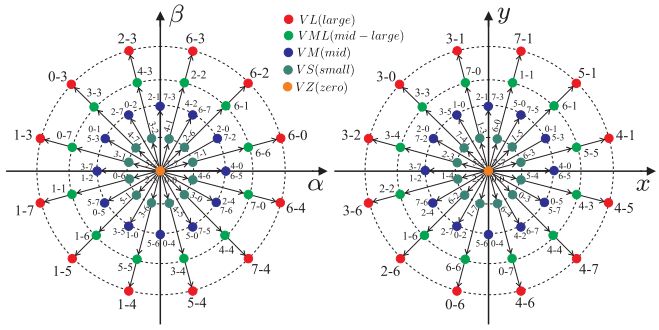

Fig. 2. Voltage space vectors of 64 switching states in $(\alpha\beta)$ and (xy) planes for the SPIM.

sampling frequency and rotor speed. Finally, Section IV concludes this article.

II. SPIM Mathematical Model

The studied system is made of a SPIM fed by a six-phase voltage source inverter (VSI) energized by a dc voltage source (V_{dc}). The electrical scheme of the six-phase VSI, based on isolated gate bipolar transistors, is illustrated in Fig. 1. The SPIM is considered as a continuous model, which can be represented by differential equations. The 6-D space of the SPIM, which is defined by its six-phases (a, b, c, d, e, f), and the vector space decomposition (VSD) technique are considered. Then, the model can be represented into three different 2-D orthogonal planes in stationary reference planes, $(\alpha-\beta)$, $(x-y)$, and (z_1-z_2), by using (1), where the invariant amplitude criteria has been considered [34]. The SPIM is asymmetrical, so it has a phase shift of 30° between the three phases and has an isolated neutral configuration. Thus, (z_1-z_2) currents are considered null

$$\mathbf{T}=\frac{1}{3}\begin{array}{c}\begin{matrix}a & d & b & e & c & f\end{matrix}\\ \begin{bmatrix}1 & \frac{\sqrt{3}}{2} & -\frac{1}{2} & -\frac{\sqrt{3}}{2} & -\frac{1}{2} & 0\\ 0 & \frac{1}{2} & \frac{\sqrt{3}}{2} & \frac{1}{2} & -\frac{\sqrt{3}}{2} & -1\\ 1 & -\frac{\sqrt{3}}{2} & -\frac{1}{2} & \frac{\sqrt{3}}{2} & -\frac{1}{2} & 0\\ 0 & \frac{1}{2} & -\frac{\sqrt{3}}{2} & \frac{1}{2} & \frac{\sqrt{3}}{2} & -1\\ 1 & 0 & 1 & 0 & 1 & 0\\ 0 & 1 & 0 & 1 & 0 & 1\end{bmatrix}\end{array}\begin{matrix}\alpha\\ \beta\\ x\\ y\\ z_1\\ z_2\end{matrix}. \tag{1}$$

The six-leg VSI has a digital output that depends on the different $2^6=64$ possible switching states defined by the six-legs. The switching states and V_{dc} determine the phase voltages, which can be drawn into $(\alpha-\beta)$ and $(x-y)$ planes according to the VSD approach [35]. Fig. 2 shows the 64 possibilities with only 49 different vectors (48 vectors + 1 null vector) in the $(\alpha-\beta)$ and $(x-y)$ planes in terms of octal nomenclature. The state-space mathematical model of the SPIM is modeled by

$$\dot{\mathbf{X}}_{(t)}=\mathbf{A}_{(t)}\,\mathbf{X}_{(t)}+\mathbf{B}_{(t)}\,\mathbf{U}_{(t)}+\mathbf{H}\,\varpi_{(t)} \tag{2}$$

where $\mathbf{X}_{(t)}=[x_1,\,x_2,\,x_3,\,x_4,x_5,\,x_6]^T$ is the state vector, which represents the stator and rotor currents $x_1=i_{\alpha s}$, $x_2=i_{\beta s}$, $x_3=i_{xs}$, $x_4=i_{ys}$, $x_5=i_{\alpha r}$ and $x_6=i_{\beta r}$, $\mathbf{U}_{(t)}=[u_1,\,u_2,\,u_3,\,u_4]^T=[v_{\alpha s},\,v_{\beta s},\,v_{xs},\,v_{ys}]^T$ is the input voltage vector applied to the stator windings, $\mathbf{H}$ represents the noise weight matrix, the process noise is considered as $\varpi_{(t)}$, and $\mathbf{A}_{(t)}$ and $\mathbf{B}_{(t)}$ are matrices defined by the electrical parameters of the SPIM as follows and also at the bottom of the next page:

$$\mathbf{B}_{(t)}=\begin{bmatrix}c_2 & 0 & 0 & 0\\ 0 & c_2 & 0 & 0\\ 0 & 0 & c_3 & 0\\ 0 & 0 & 0 & c_3\\ -c_4 & 0 & 0 & 0\\ 0 & -c_4 & 0 & 0\end{bmatrix}$$

where R_s, R_r, L_m, $L_r=L_{lr}+L_m$, and $L_s=L_{ls}+L_m$ are the electrical parameters of the SPIM. The coefficients are considered as $c_1=L_sL_r-L_m^2$, $c_2=\frac{L_r}{c_1}$, $c_3=\frac{1}{L_{ls}}$, $c_4=\frac{L_m}{c_1}$, and $c_5=\frac{L_s}{c_1}$. Stator voltages are dependant on the input control signals $\mathbf{S}$, which is considered the actual switching state. For this analysis, the ideal VSI has been modeled to obtain a good optimization process. The stator voltages can be calculated from the ideal six-leg VSI model $\mathbf{M}_{[\mathbf{S}]}$ [34]

$$\mathbf{M}_{[\mathbf{S}]}=\frac{1}{3}\begin{bmatrix}2 & 0 & -1 & 0 & -1 & 0\\ 0 & 2 & 0 & -1 & 0 & -1\\ -1 & 0 & 2 & 0 & -1 & 0\\ 0 & -1 & 0 & 2 & 0 & -1\\ -1 & 0 & -1 & 0 & 2 & 0\\ 0 & -1 & 0 & -1 & 0 & 2\end{bmatrix}\mathbf{S}^T \tag{3}$$

where $\mathbf{S}=[S_a,\,S_d,\,S_b,\,S_e,\,S_c,\,S_f]$ and $\mathbf{S}_i\in\{0,1\}$. The ideal six-phase VSI generates the stator voltages through the switching gating signals and V_{dc} and then they are transformed to $(\alpha\beta)$ and (xy) planes, represented by $\mathbf{U}_{(t)}$, calculated in the following equation:

$$\mathbf{U}_{(t)}=V_{dc}\,\mathbf{T}\,\mathbf{M}_{[\mathbf{S}]}. \tag{4}$$

The output vector $\mathbf{Y}$ is

$$\mathbf{Y}_{(t)}=\mathbf{C}\,\mathbf{X}_{(t)}+\nu_{(t)} \tag{5}$$

where $\nu_{(t)}$ is the measurement noise and $\mathbf{C}$ is considered as follows:

$$\mathbf{C}=\begin{bmatrix}1 & 0 & 0 & 0 & 0 & 0\\ 0 & 1 & 0 & 0 & 0 & 0\\ 0 & 0 & 1 & 0 & 0 & 0\\ 0 & 0 & 0 & 1 & 0 & 0\end{bmatrix}.$$

The mechanical variables of the SPIM are considered in the following equations:

$$T_e = 3\,P\,(\psi_{\alpha s} i_{\beta s} - \psi_{\beta s} i_{\alpha s}) \tag{6}$$

$$J_i\,\dot{\omega}_m + B_i\,\omega_m = (T_e - T_L) \tag{7}$$

$$\omega_r = P\omega_m \tag{8}$$

where T_e represents the electromagnetic torque, P the number of pole pairs, $\psi_{\alpha s}$ and $\psi_{\beta s}$ are considered the stator fluxes, J_i is the inertia coefficient, B_i is considered the friction coefficient, T_L is the load torque, ω_r is the rotor electrical angular speed, and ω_m is the rotor mechanical speed.

III. Traditional PCC and Its Variants

The mathematical model of the SPIM (2) and (5) has to be discretized so it can be considered for the PCC. A forward-Euler method is computed to avoid a high computational cost for the digital controller. The equations will then be in a discrete form with the future variables only depending on past values of the variables and not on present values. Thus, a prediction of the future (next sample state) $\hat{\mathbf{X}}_{[k+1|k]}$ is written as

$$\hat{\mathbf{X}}_{[k+1|k]} = \mathbf{X}_{[k]} + \mathrm{f}\left(\mathbf{X}_{[k]},\, \mathbf{U}_{[k]},\, T_s,\, \boldsymbol{\omega}_{r[k]}\right) \tag{9}$$

where $[k]$ is the current sample and T_s the sampling time. Fig. 3 presents the block diagram of the system with the SPIM and the analyzed current controllers.

A. Rotor Currents Observer

Stator currents and mechanical rotor speed are the only measured variables in the state-space model (9). On the other hand, stator voltages can be calculated from the switching states sent to the VSI. However, rotor currents cannot be easily measured in a real system and they have to be estimated. This can be solved by reduced-order observers of rotor currents. The reduced-order observers only estimate the value of the unmeasured parts of the state vector. The latter is an important issue that has been already solved by using Luenberger observer (LO) [36] and Kalman filter (KF) [37], [38]. KF is considered a superior option because their observer gains are estimated and optimized in every sampling time by considering the noise input in the system. For LO, gains are not so optimized and the setting is deterministic [37]. Therefore, KF is considered and implemented in this article to improve the control performance of PCC by reducing the prediction errors. Zero-mean Gaussian measurement noises and uncorrelated processes are considered. Now, the predictive model of the SPIM in state-space representation is defined as follows:

$$\hat{\mathbf{X}}_{[k+1|k]} = \mathbf{A}_{[k]}\mathbf{X}_{[k]} + \mathbf{B}_{[k]}\mathbf{U}_{[k]} + \mathbf{H}\varpi_{[k]} \tag{10}$$

$$\mathbf{Y}_{[k+1|k]} = \mathbf{C}\,\mathbf{X}_{[k+1]} + \nu_{[k+1]} \tag{11}$$

where $\mathbf{A}_{[k]}$ and $\mathbf{B}_{[k]}$ are matrices defined by (12)–(15). $\mathbf{A}_{[k]}$ also depends on the actual value of $\omega_{r[k]}$ and has to be computed at every sampling time. A more detailed explanation of the error convergence of the KF and its dynamics are described in [37] and [38]. The system matrices are defined as

$$\mathbf{A}_{[k]} = \begin{bmatrix} A_{11} & A_{12} & 0 & 0 & A_{15} & A_{16} \\ A_{21} & A_{22} & 0 & 0 & A_{25} & A_{26} \\ 0 & 0 & A_{33} & 0 & 0 & 0 \\ 0 & 0 & 0 & A_{44} & 0 & 0 \\ A_{51} & A_{52} & 0 & 0 & A_{55} & A_{56} \\ A_{61} & A_{62} & 0 & 0 & A_{65} & A_{66} \end{bmatrix} \tag{12}$$

where $\mathbf{A}_{[k]}$ parameters are

$$\begin{aligned} A_{11} &= A_{22} = 1 - T_s c_2 R_s \\ A_{12} &= -A_{21} = T_s c_4 L_m \omega_{r[k]} \\ A_{15} &= A_{26} = T_s c_4 R_r \\ A_{16} &= -A_{25} = T_s c_4 L_r \omega_{r[k]} \\ A_{33} &= A_{44} = 1 - T_s c_3 R_s \\ A_{51} &= A_{62} = -T_s c_4 R_s \\ A_{52} &= -A_{61} = -T_s c_5 L_m \omega_{r[k]} \\ A_{55} &= A_{66} = 1 - T_s c_5 R_r \\ A_{56} &= -A_{65} = -c_5 \omega_{r[k]} T_s L_r \end{aligned} \tag{13}$$

$$\mathbf{B}_{[k]} = \begin{bmatrix} B_{11} & 0 & 0 & 0 & 0 & 0 \\ 0 & B_{22} & 0 & 0 & 0 & 0 \\ 0 & 0 & B_{33} & 0 & 0 & 0 \\ 0 & 0 & 0 & B_{44} & 0 & 0 \\ 0 & 0 & 0 & 0 & B_{55} & 0 \\ 0 & 0 & 0 & 0 & 0 & B_{66} \end{bmatrix} \tag{14}$$

being $\mathbf{B}_{[k]}$ parameters

$$\begin{aligned} B_{11} &= B_{22} = T_s c_2 \\ B_{33} &= B_{44} = T_s c_3 \\ B_{55} &= B_{66} = -T_s c_4. \end{aligned} \tag{15}$$

$$\mathbf{A}_{(t)} = \begin{bmatrix} -R_s c_2 & c_4 L_m \omega_r & 0 & 0 & c_4 R_r & c_4 L_r \omega_r \\ c_4 L_m \omega_r & -R_s c_2 & 0 & 0 & c_4 L_r \omega_r & c_4 R_r \\ 0 & 0 & -R_s c_3 & 0 & 0 & 0 \\ 0 & 0 & 0 & -R_s c_3 & 0 & 0 \\ R_s c_4 & -c_5 L_m \omega_r & 0 & 0 & -c_5 R_r & -c_5 L_r \\ -c_5 L_m \omega_r & R_s c_4 & 0 & 0 & -c_5 L_r & -c_5 R_r \end{bmatrix}$$

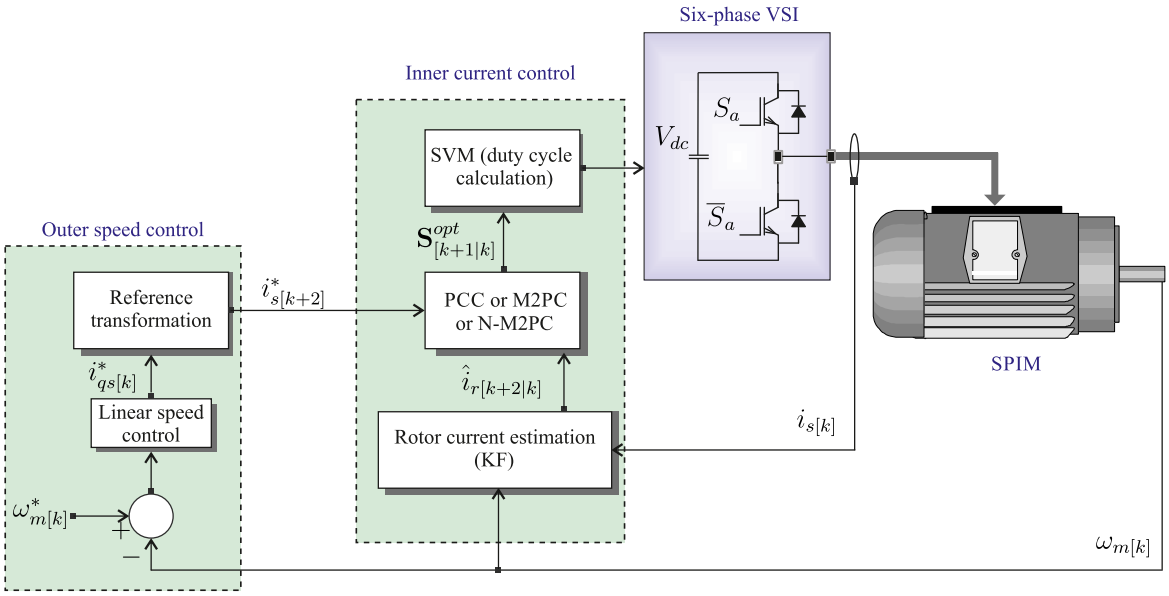

Fig. 3. Block diagram of the controlled system based on FOC and traditional PCC, M2PC, and N-M2PC.

B. Cost Function Minimization

The cost function is considered as an optimization process of different system variables such as harmonic content minimization, machine torque ripple minimization, VSI switching losses, and current tracking error [39]. This last variable is the most important figure of merit in PCC in $(\alpha\beta)$ and (xy) planes. PCC evaluates the cost function for 49 iterations regarding 49 different voltage vectors. Therefore, the selected cost function is

$$J_{[k+2|k]} = \Big[(i^*_{\alpha s[k+2]} - \hat{i}_{\alpha s[k+2|k]})^2 + (i^*_{\beta s[k+2]} - \hat{i}_{\beta s[k+2|k]})^2 + \lambda_{xy} \left((i^*_{xs[k+2]} - \hat{i}_{xs[k+2|k]})^2 + (i^*_{ys[k+2]} - \hat{i}_{ys[k+2|k]})^2 \right) \Big]^{\frac{1}{2}}. \quad (16)$$

A second-step ahead prediction of stator currents $\hat{i}_{s[k+2|k]}$ is computed for delay compensation, by considering (10) and (11). The desired reference trajectory of the stator currents is represented by $i^*_{s[k+2]}$. The weighting factor optimization is tackled in [40]. Typically, for SPIM, λ_{xy} gives more priority to stator currents in $(\alpha\beta)$ plane than (xy) to prioritize the flux/torque production plane over the machine losses [37].

C. Modulated Model Predictive Control

This PCC with a modulation stage consists on determine each available sector for the six-leg VSI in the $(\alpha\beta)$ plane, being 12 outside sectors in total, which are composed of two adjacent active vectors and the null vector (VZ), as shown in Fig. 4. Then, it calculates the future prediction of the three vectors at every sampling time and analyses their respective cost functions (J_0, J_1, and J_2) separately. This technique can generate any voltage vector in the $(\alpha\beta)$ plane using the large vectors (VL) and VZ, covering the entire space vector area. It can be noted that VL are

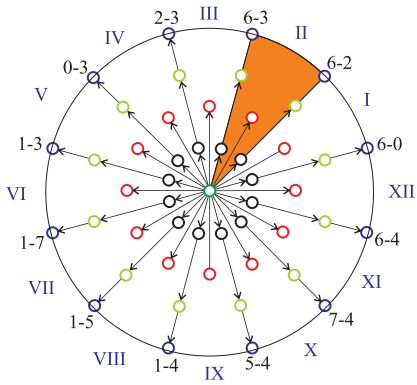

Fig. 4. Space voltage sectors of M2PC.

the smallest voltage vectors in (xy) plane, managing a natural reduction of $(x-y)$ currents [26].

The duty cycles (d_0, d_1, and d_2) are obtained by solving the following equations:

$$d_0 = \frac{\gamma}{J_0} \quad d_1 = \frac{\gamma}{J_1} \quad d_2 = \frac{\gamma}{J_2} \quad (17)$$

$$d_0 + d_1 + d_2 = T_s. \quad (18)$$

The duty cycles for each vector are given as

$$J_T = J_1 J_2 + J_0 J_1 + J_0 J_2 \quad (19)$$

$$d_0 = \frac{T_s J_1 J_2}{J_T} \quad (20)$$

$$d_1 = \frac{T_s J_0 J_2}{J_T} \quad (21)$$

$$d_2 = \frac{T_s J_0 J_1}{J_T}. \quad (22)$$

At last, the selected sector cost function is considered as

$$G_{[k+2|k]} = d_1 J_1 + d_2 J_2. \tag{23}$$

The sector, which reduces $G_{[k+2|k]}$, is applied to the six-leg VSI at the next sampling time. It is necessary to synthesize the duty cycles, to be able to implement a symmetric pulsewidth modulation (PWM) as follows:

$$\tau_{(i)} = \frac{d_0}{2T_s} + \frac{d_1}{T_s} v_{1(i)} + \frac{d_2}{T_s} v_{2(i)} \tag{24}$$

where $i = [a, d, b, e, c, f]$ and τ_i is the PWM duty cycle per leg, obtaining a fixed switching frequency.

D. N-M2PC

The main difference between N-M2PC and M2PC is the shape of each voltage sector. M2PC uses two VL and VZ per sector and N-M2PC uses four including two mid vectors (VM) and two VL. As in M2PC, 12 rectangular sectors are considered and their respective cost functions (J_1, J_2, J_3, and J_4) are calculated separately at every sampling time. The main goal of this modulation is to reduce the steady-state error of the stator currents tracking in (dq) plane by including these adjacent VM per sector avoiding the use of VZ, which limits the voltage range, reducing the tracking capacity of the stator currents in ($\alpha\beta$) plane, since VZ has an increased duty cycle when ($x - y$) currents are being reduced [27].

The duty cycles, for VL and VM d_1, d_2, d_3, and d_4, are obtained as follows:

$$d_1 = \frac{\gamma}{J_1} \quad d_2 = \frac{\gamma}{J_2} \quad d_3 = \frac{\gamma}{J_3} \quad d_4 = \frac{\gamma}{J_4} \tag{25}$$

$$d_1 + d_2 + d_3 + d_4 = T_s \tag{26}$$

where J_1, J_2, J_3, and J_4 are the corresponding cost functions (16) for the four vectors and γ is an auxiliary variable whose value depends directly on the cost function values. Then, the duty cycles for each vector are calculated as

$$J_{T1} = J_1 J_3 J_4 + J_2 J_3 J_4 \tag{27}$$

$$J_{T2} = J_1 J_2 J_4 + J_1 J_2 J_3 \tag{28}$$

$$d_1 = \frac{T_s J_2 J_3 J_4}{J_{T1} + J_{T2}} \tag{29}$$

$$d_2 = \frac{T_s J_1 J_3 J_4}{J_{T1} + J_{T2}} \tag{30}$$

$$d_3 = \frac{T_s J_1 J_2 J_4}{J_{T1} + J_{T2}} \tag{31}$$

$$d_4 = \frac{T_s J_1 J_2 J_3}{J_{T1} + J_{T2}}. \tag{32}$$

At last, the final cost function is computed as

$$G_{[k+2|k]} = d_1 J_1 + d_2 J_2 + d_3 J_3 + d_4 J_4. \tag{33}$$

As in M2PC, the sector which reduces $G_{[k+2|k]}$ the most is applied to the six-leg VSI at the next sampling time with their respective duty cycles for every vector (mid and large) in the selected sector. A simple equation is used to obtain the duty cycles $\tau_{(i)}$ for the switching devices of each phase of the six-leg VSI, as follows:

$$\tau_{(i)} = \frac{d_1}{T_s} v_{1(i)} + \frac{d_2}{T_s} v_{2(i)} + \frac{d_3}{T_s} v_{3(i)} + \frac{d_4}{T_s} v_{4(i)} \tag{34}$$

where $\tau_{(i)}$ is normalized between 0 and 1, for the switching devices for the six-leg VSI.

TABLE I
RANGE VALUES OF DIFFERENT GAINS ($\mathbf{L}_{[k]}$) OF M2PC AND N-M2PC

Gains	M2PC	N-M2PC
L_1	$[-10, 10]$	$[-10, 10]$
L_2	$[-40, 40]$	$[-40, 40]$
L_3	$[-150, 10]$	$[-760, -300]$
L_4	$[-40, 40]$	$[-40, 40]$

IV. PRACTICAL STABILITY STUDY

Examples of PCC variants are vastly known in the literature, which present some common properties and allow them to formalize the stability analysis [41]. A candidate-Lyapunov function is often considered as a popular method to prove the stability of PCC. Another considered approach, presented in [23] and[42] consists in estimate a specific gain $\mathbf{L}_{[k]}$ to obtain a stable matrix $(\mathbf{A}_{[k]} - \mathbf{B}_{[k]}\mathbf{L}_{[k]})$ whose eigenvalues are less than 1. The second method is more practical due to its simplicity and by considering that PCC has a finite control effort, i.e., 49 voltage vectors in the particular case of the SPIM. For a limited current reference (due to security issues), there is a finite number of $\mathbf{L}_{[k]}$ through the cost function minimization and it shows the same behavior in terms of local stability by analyzing different scenarios, such as typical values of rotor speed and sampling frequency (F_s)

$$\mathbf{U}_{[k]} = -\mathbf{L}_{[k]}\mathbf{X}_{[k]} \tag{35}$$

where $\mathbf{L}_{[k]}$ is selected as follows:

$$\mathbf{L}_{[k]} = \begin{bmatrix} L_1 & L_2 & 0 & 0 & L_3 & L_4 \\ -L_2 & L_1 & 0 & 0 & -L_4 & L_3 \\ 0 & 0 & L_1 & L_2 & 0 & 0 \\ 0 & 0 & -L_2 & L_1 & 0 & 0 \end{bmatrix}.$$

It is considered a limited range of $[-3.5, 3.5]$ A, by considering the nominal current value of the SPIM, for state variables ($\mathbf{X}_{[k]}$). Then, by using the separation theorem, the closed-loop eigenvalues are the union of those of the observer and state feedback. Assuming measured states, and finite values of the voltage vector ($\mathbf{U}_{[k]}$), i.e., 49 different values for traditional PCC, a finite number of $\mathbf{L}_{[k]}$ is found through an exhaustive iterative search, as shown in Table I. It is worth mentioning that $\mathbf{L}_{[k]}$ can be defined with infinite different values, so bounded ranges of values for every parameter of $\mathbf{L}_{[k]}$ are considered. It is also noted that PCC is a constraint optimal control method, therefore, the selected control effort should be stable as long as inside the solution region at least one stable solution exists (inside the unit circle). Thus, rotor speed values are increased to obtain unstable solutions, and this value is defined as the upper bound of stable rotor speed. At the same time, Table II

TABLE II
STABILITY THEORETICAL ANALYSIS OF M2PC AND N-M2PC AND THEIR MAXIMUM STABLE SPEEDS (R/MIN)

F_s (kHz)	M2PC	N-M2PC
	Maximum Stable Speed	
2	850	250
2.5	1000	550
4	1300	1250
5	1400	1650
7.5	1700	2800
8	1850	2850
10	2000	3000
12.5	2300	3000
15	2600	3000
16	2700	3000
17.5	2800	3000
20	3000	3000

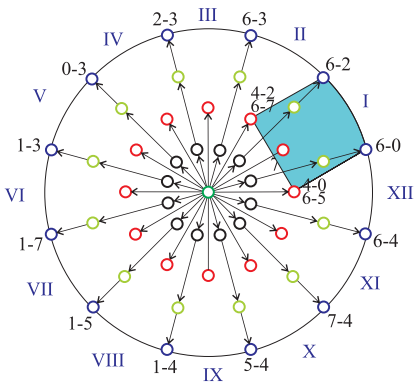

Fig. 5. Space voltage sectors of N-M2PC.

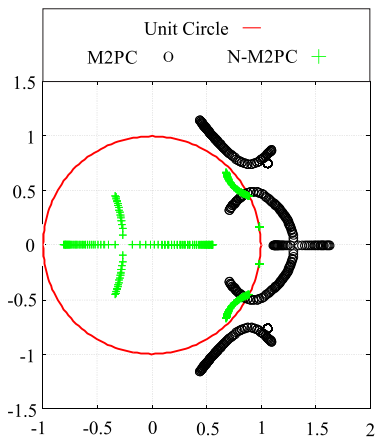

Fig. 6. Eigenvalues of $(\mathbf{A}_{[k]} - \mathbf{B}_{[k]}\mathbf{L}_{[k]})$ matrix at 10 kHz of sampling frequency and rotor speed of 2500 r/min for M2PC and N-M2PC.

presents the maximum stable rotor speed (eigenvalues inside the unit circle) at different sampling frequencies for M2PC and N-M2PC. The theoretical analysis is only considered for M2PC and N-M2PC since they are the main MPCC schemes studying in this article. At last, eigenvalues of $(\mathbf{A}_{[k]} - \mathbf{B}_{[k]}\mathbf{L}_{[k]})$ matrix at 10 kHz of sampling frequency and rotor speed of 2500 r/min for the three techniques are shown in Fig. 6 where, at those conditions, N-M2PC is the only controller with eigenvalues inside the unit circle.

TABLE III
PARAMETERS OF THE SPIM

PARAMETER	VALUE	PARAMETER	VALUE
R_r (Ω)	6.9	R_s (Ω)	6.7
L_s (mH)	654.4	L_r (mH)	626.8
L_m (mH)	614	L_{ls} (mH)	5.3
ω_{m-nom} (rpm)	2 540	P_w (kW)	2
J_i (kg.m^2)	0.07	B_i (kg.m^2/s)	0.0004
P	1	V_{dc} (V)	700

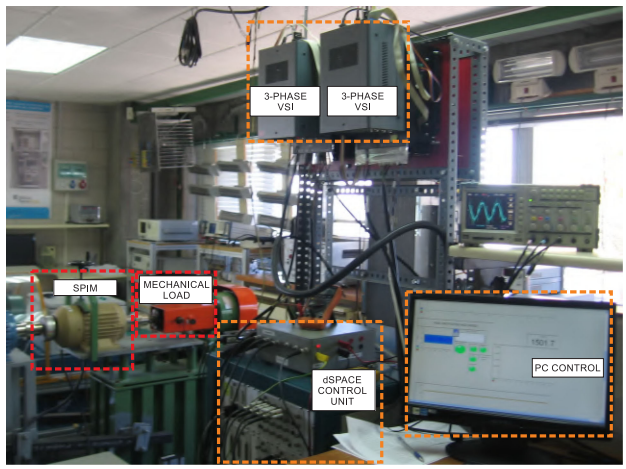

Fig. 7. Setup of the experimental test bench including the dSPACE platform, the SPIM, the six-phase VSI, and the eddy current brake.

V. EXPERIMENTAL RESULTS

The stability analysis is validated through experimental tests for traditional PCC, M2PC, and N-M2PC in the experimental test bench. It must be considered that despite not presenting theoretical results for the traditional PCC, experimental tests were carried out to have a comparative pattern.

A. Experimental Test Bench

The experimental test bench is composed of a SPIM fed by two conventional three-phase VSI, using a dc voltage source. The six-phase VSI is controlled by a real-time rapid prototyping platform defined as dSPACE MABXII DS1401, with MATLAB/Simulink incorporated. Table III presents the parameters of the SPIM obtained using stand-still VSI tests and typical methods of ac time domain [43], [44].

The measurements were made with current sensors LA 55-P s, with many turns to improve the precision at low current amplitude. They also have a frequency bandwidth from dc up to 200 kHz. The data are converted to digital through a 16-bit A/D converter. The SPIM rotor angle is obtained by a 1024 ppr incremental encoder and the rotor speed is estimated from the angle. At last, a 5 HP eddy current brake is selected as a variable mechanical load on the SPIM, which is considered at 1 A, generating a load torque of 1.5 Nm. A block diagram of the experimental test bench is shown in Fig. 7. The cost function

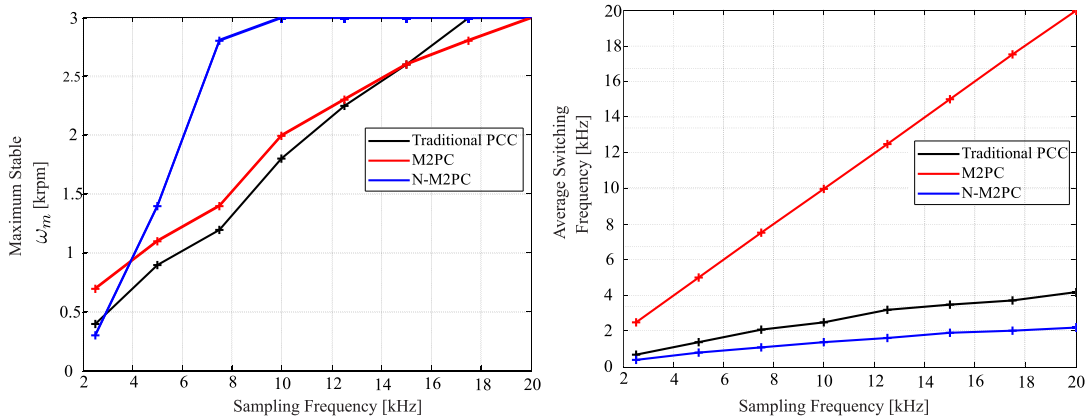

Fig. 8. Trend chart of traditional PCC, M2PC, and N-M2PC regarding different sampling frequencies and: (a) rotor mechanical speed; (b) average switching frequency.

in (16) with $\lambda_{xy} = 0.05$ is considered to apply the traditional PCC and M2PC. This gives priority to $(\alpha - \beta)$ stator currents tracking over $(x - y)$ currents reduction. As for N-M2PC, $\lambda_{xy} = 0.1$ is selected because the null vector is not used and hence $(x - y)$ currents reduction is obtained through combination of the active vectors. It is worth mentioning that λ_{xy} does not influence the maximum stable rotor speed, it only affects the performance of the currents tracking in a range of $[0.01, 0.1]$, which are the tested values. These values of λ_{xy} were obtained through a heuristic method, which consists in a manual tuning checked by trial and error, by focusing on obtaining a suboptimal system [37]. The covariances of the process $(\varpi_{(t)})$ and measurement $(\nu_{(t)})$ noises, defined as $\hat{Q}_w = 0.0022$ and $\hat{R}_v = 0.0022$, can be estimated by using the proposed method in [38].

B. Stability Test

In every case, $(x - y)$ current references are considered zero $(i^*_{xs} = i^*_{ys} = 0)$. Then, a fixed d stator current $(i^*_{ds} = 1$ A) has been set. The sampling frequencies, in the tests, are 2.5, 5, 7.5, 10, 12.5, 15, 17.5, and 20 kHz. Fig. 8(a) and (b) shows the trend charts of the maximum stable rotor speeds, which is defined as the rotor speed where the stator currents controller can no longer regulate properly as larger oscillations appear destabilizing the system, and average switching frequencies for traditional PCC [37], M2PC, and N-M2PC at different sampling frequencies. The results show that N-M2PC has the best performance regarding local stability with the maximum rotor speed of the SPIM, where at lower sampling frequency the performance is not much different to traditional PCC and M2PC although at higher sampling frequency, N-M2PC can operate in the entire speed range of the machine, as for traditional PCC and M2PC, they tend to improve linearly local stability at higher sampling frequency where traditional PCC has a steep slope compared to M2PC. As for average switching frequency, M2PC is a fixed switching frequency technique, so it matches the switching frequency and the sampling frequency. However, traditional PCC and N-M2PC are variable switching frequency techniques, thus the switching states will not necessarily change in two consecutive sampling times, thus, the average switching frequencies are lower where N-M2PC has almost half the average switching frequency than traditional PCC, having different pulse ratios under equivalent conditions, increasing the total harmonic distortion of stator currents but reducing the switching losses in the six-phase VSI, as shown in [27], as well as the $(x - y)$ currents reduction.

TABLE IV
OPTIMAL VOLTAGE VECTORS AND THEIR CORRESPONDING DUTY CYCLES FOR M2PC AND N-M2PC FOR CONSECUTIVE SAMPLING PERIODS

M2PC			
Sample	Vector	Switching State	Duty Cycle
1	v_0	0-0	$d_0 = 0.3572T_s$
1	v_1	1-5	$d_1 = 0.3082T_s$
1	v_2	1-7	$d_2 = 0.3346T_s$
2	v_0	0-0	$d_0 = 0.3052T_s$
2	v_1	1-4	$d_1 = 0.4456T_s$
2	v_2	1-5	$d_2 = 0.2492T_s$
3	v_0	0-0	$d_0 = 0.2876T_s$
3	v_1	1-4	$d_1 = 0.3441T_s$
3	v_2	1-5	$d_2 = 0.3683T_s$
N-M2PC			
Sample	Vector	Switching State	Duty Cycle
1	v_1	0-2	$d_1 = 0.1562T_s$
1	v_2	2-3	$d_2 = 0.2586T_s$
1	v_3	6-3	$d_3 = 0.4085T_s$
1	v_4	6-7	$d_4 = 0.1767T_s$
2	v_1	0-1	$d_1 = 0.1727T_s$
2	v_2	0-3	$d_2 = 0.5216T_s$
2	v_3	2-3	$d_3 = 0.1781T_s$
2	v_4	7-3	$d_4 = 0.1276T_s$
3	v_1	0-1	$d_1 = 0.2151T_s$
3	v_2	0-3	$d_2 = 0.4275T_s$
3	v_3	2-3	$d_3 = 0.2010T_s$
3	v_4	7-3	$d_4 = 0.1564T_s$

On the other hand, Table IV presents the selected voltage vectors and their respective duty cycles calculated in consecutive sampling periods for M2PC and N-M2PC showing the performance of both modulated techniques. Then, Fig. 9(a) and (b) presents the dynamic behavior of the rotor speed and stator currents at a stable critical condition for N-M2PC, where

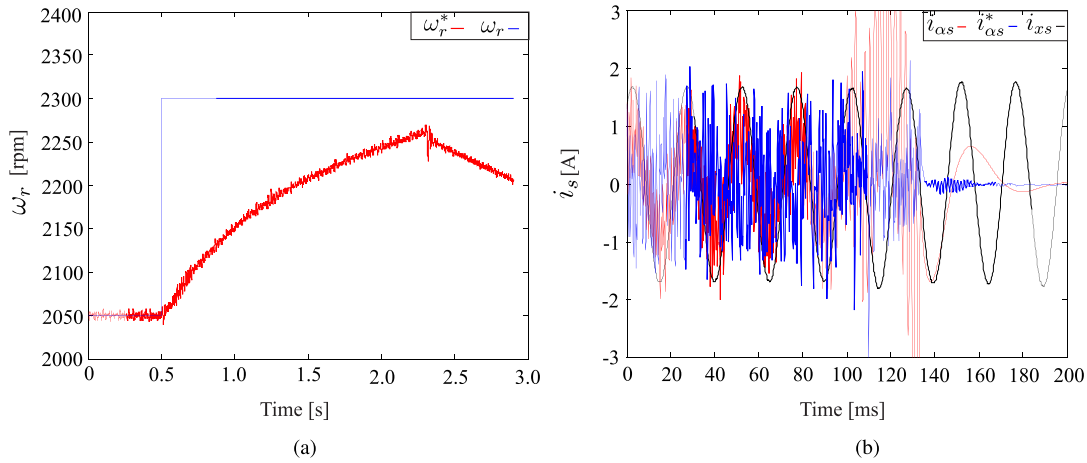

Fig. 9. Dynamic results of rotor speed and stator currents for N-M2PC at a critical stable condition with 2250 r/min and a sampling frequency of 6 kHz: (a) rotor mechanical speed; (b) stator currents.

TABLE V
RELATIVE ERROR (%) BETWEEN THEORETICAL AND EXPERIMENTAL MAXIMUM STABLE ROTOR SPEEDS M2PC AND N-M2PC AND THEIR MAXIMUM STABLE SPEEDS (R/MIN)

F_s (kHz)	M2PC	N-M2PC
	Error of Maximum Stable Speed	
2.5	30.0	45.5
5	21.4	15.2
7.5	17.6	0.0
10	0.0	0.0
12.5	2.2	0.0
15	0.0	0.0
17.5	0.0	0.0
20	0.0	0.0

the measured speed shows oscillations tend to destabilize the system, then the electrical protections are activated. Finally, Table V shows the relative error between theoretical and experimental maximum stable rotor speeds obtained at different sampling frequencies for M2PC and N-M2PC. The relative error is significantly low, especially a higher speeds where it matches almost perfectly. However, a difference between the results at low sampling frequencies can be observed as well as a nonlinear behavior between the sampling frequency and the error variation. This can be explained if it is considered that the model parameters have errors that are accentuated with low sampling frequencies since a greater current ripple is generated, degrading the signal-to-noise ratio. In addition, the transport delay of the converter is greater. All these aforementioned aspects are not considered in the theoretical analysis. Even so, a clear trend of the relationship between the sampling frequency and the maximum stable rotor speed can be observed.

VI. CONCLUSION

This article has proposed a practical stability study for modulated model predictive controllers applied to an asymmetrical SPIM. The experimental results validated the limits of stability regarding rotor speed and sampling frequencies for the modulated PCCs. From an engineering point of view, a way to obtain these critical operating values can be appreciated in order to apply modulated PCC techniques with the lowest possible sampling frequency, which reduce the switching losses in power converters. It was shown an approximately linear relationship between the maximum rotor speed and the sampling frequency and the theoretical analysis showed a very similar behavior by considering a finite range of gains, which represent the different current controllers, even for N-M2PC as shown for frequencies less than 7.5 kHz, although it can be considered that this trend maintains for higher frequencies, it would be necessary to work with speeds higher than 3000 r/min and it is out of the scope of this article, validating the proposed method, which can be applied to other systems with PCC.

REFERENCES

[1] P. Gonçalves, S. Cruz, and A. Mendes, "Finite control set model predictive control of six-phase asymmetrical machines-an overview," *Energies*, vol. 12, no. 24, 2019, Art no. 4693.
[2] I. Gonzalez-Prieto, M. J. Duran, J. J. Aciego, C. Martin, and F. Barrero, "Model predictive control of six-phase induction motor drives using virtual voltage vectors," *IEEE Trans. Ind. Electron.*, vol. 65, no. 1, pp. 27–37, Jan. 2018.
[3] S. Vazquez, J. Rodriguez, M. Rivera, L. G. Franquelo, and M. Norambuena, "Model predictive control for power converters and drives: Advances and trends," *IEEE Trans. Ind. Electron.*, vol. 64, no. 2, pp. 935–947, Feb. 2017.
[4] S. Paul and K. Basu, "A three-phase inverter based overmodulation strategy of asymmetrical six-phase induction machine," *IEEE Trans. Power Electron.*, vol. 36, no. 5, pp. 5802–5817, May 2021.
[5] F. Barrero, M. R. Arahal, R. Gregor, S. Toral, and M. J. Durán, "A proof of concept study of predictive current control for VSI-driven asymmetrical dual three-phase AC machines," *IEEE Trans. Ind. Electron.*, vol. 56, no. 6, pp. 1937–1954, Jun. 2009.
[6] F. Barrero *et al.*, "An enhanced predictive current control method for asymmetrical six-phase motor drives," *IEEE Trans. Ind. Electron.*, vol. 58, no. 8, pp. 3242–3252, Aug. 2011.
[7] C. S. Lim, E. Levi, M. Jones, N. A. Rahim, and W. P. Hew, "FCS-MPC-based current control of a five-phase induction motor and its comparison with PI-PWM control," *IEEE Trans. Ind. Electron.*, vol. 61, no. 1, pp. 149–163, Jan. 2014.
[8] E. Levi, "Advances in converter control and innovative exploitation of additional degrees of freedom for multiphase machines," *IEEE Trans. Ind. Electron.*, vol. 63, no. 1, pp. 433–448, Jan. 2016.

[9] F. Barrero and M. J. Duran, "Recent advances in the design, modeling, and control of multiphase machines: Part I," *IEEE Trans. Ind. Electron.*, vol. 63, no. 1, pp. 449–458, Jan. 2016.
[10] H. S. Che, M. J. Duran, E. Levi, M. Jones, W.-P. Hew, and N. A. Rahim, "Postfault operation of an asymmetrical six-phase induction machine with single and two isolated neutral points," *IEEE Trans. Power Electron.*, vol. 29, no. 10, pp. 5406–5416, Oct. 2014.
[11] A. G. Yepes, J. Doval-Gandoy, and H. A. Toliyat, "Strategy with smooth transitions and improved torque-speed region and stator copper loss for two-level asymmetrical six-phase induction motor drives under switch faults," *IEEE Trans. Power Electron.*, vol. 36, no. 2, pp. 1954–1969, Feb. 2021.
[12] G. Sala, M. Mengoni, G. Rizzoli, M. Degano, L. Zarri, and A. Tani, "Impact of star connection layouts on the control of multiphase induction motor drives under open-phase fault," *IEEE Trans. Power Electron.*, vol. 36, no. 4, pp. 3717–3726, Apr. 2021.
[13] M. J. Duran and F. Barrero, "Recent advances in the design, modeling, and control of multiphase machines: Part II," *IEEE Trans. Ind. Electron.*, vol. 63, no. 1, pp. 459–468, Jan. 2016.
[14] I. Subotic, N. Bodo, E. Levi, B. Dumnic, D. Milicevic, and V. Katic, "Overview of fast on-board integrated battery chargers for electric vehicles based on multiphase machines and power electronics," *Elect. Power Appl.*, vol. 10, no. 3, pp. 217–229, 2016.
[15] Y. Kali *et al.*, "Current control of a six-phase induction machine drive based on discrete-time sliding mode with time delay estimation," *Energies*, vol. 12, no. 1, p. 170–186, 2019, doi: 10.3390/en12010170.
[16] Y. Kali *et al.*, "Time delay estimation based discrete-time super-twisting current control for a six-phase induction motor," *IEEE Trans. Power Electron.*, vol. 35, no. 11, pp. 12570–12580, Nov. 2020
[17] M. A. Fnaiech, F. Betin, G.-A. Capolino, and F. Fnaiech, "Fuzzy logic and sliding-mode controls applied to six-phase induction machine with open phases," *IEEE Trans. Ind. Electron.*, vol. 57, no. 1, pp. 354–364, Jan. 2010.
[18] Z. Liu, Z. Zheng, and Y. Li, "Enhancing fault-tolerant ability of a nine-phase induction motor drive system using fuzzy logic current controllers," *IEEE Trans. Energy Conv.*, vol. 32, no. 2, pp. 759–769, Jun. 2017.
[19] M. Morawiec, P. Strankowski, A. Lewicki, J. Guziński, and F. Wilczyński, "Feedback control of multiphase induction machines with backstepping technique," *IEEE Trans. Ind. Electron.*, vol. 67, no. 6, pp. 4305–4314, Jun. 2020.
[20] Y. Kali, J. Rodas, M. Saad, J. Doval-Gandoy, and R. Gregor, "Nonlinear backstepping with time delay estimation for six-phase induction machine," in *Proc. IEEE Int. Electric Mach. Drives Conf.*, 2019, pp. 1798–1804.
[21] Y. Wang, J. Yang, S. Li, G. Yang, R. Deng, and H. Hussain, "Multiplane rotor resistance online estimation strategy for multiphase induction machine under non-sinusoidal power supply," *IEEE Trans. Power Electron.*, vol. 36, no. 8, pp. 9487–9500, Aug. 2021.
[22] J. J. Aciego, I. G. Prieto, and M. J. Duran, "Model predictive control of six-phase induction motor drives using two virtual voltage vectors," *IEEE Trans. Emerg. Sel. Topics Power Electron.*, vol. 7, no. 1, pp. 321–330, Mar. 2019.
[23] M. Ayala, J. Doval-Gandoy, J. Rodas, O. Gonzalez, and R. Gregor, "Current control designed with model based predictive control for six-phase motor drives," *ISA Trans.*, vol. 98, pp. 496–504, 2020.
[24] I. González-Prieto, M. Durán, M. Bermúdez, F. Barrero, and C. Martín, "Assessment of virtual-voltage-based model predictive controllers in six-phase drives under open-phase faults," *IEEE Trans. Emerg. Sel. Topics Power Electron.*, vol. 8, no. 3, pp. 2634–2644, Sep. 2020.
[25] M. Bermúdez, C. Martín, I. González-Prieto, M. J. Durán, M. R. Arahal, and F. Barrero, "Predictive current control in electrical drives: An illustrated review with case examples using a five-phase induction motor drive with distributed windings," *IET Electric Power Appl.*, vol. 14, no. 8, pp. 1291–1310, 2020.
[26] O. Gonzalez, M. Ayala, J. Doval-Gandoy, J. Rodas, R. Gregor, and M. Rivera, "Predictive-fixed switching current control strategy applied to six-phase induction machine," *Energies*, vol. 12, no. 12, 2019, Art. no. 2294.
[27] M. Ayala, J. Doval-Gandoy, J. Rodas, O. Gonzalez, R. Gregor, and M. Rivera, "A novel modulated model predictive control applied to six-phase induction motor drives," *IEEE Trans. Ind. Electron.*, vol. 68, no. 5, pp. 3672–3682, May 2021.
[28] M. Morari and J. H. Lee, "Model predictive control: Past, present and future," *Comput. Chem. Eng.*, vol. 23, no. 4/5, pp. 667–682, 1999.
[29] R. P. Aguilera and D. E. Quevedo, "Predictive control of power converters: Designs with guaranteed performance," *IEEE Trans. Ind. Inform.*, vol. 11, no. 1, pp. 53–63, Feb. 2015.
[30] M. Preindl, "Robust control invariant sets and Lyapunov-based MPC for IPM synchronous motor drives," *IEEE Trans. Ind. Electron.*, vol. 63, no. 6, pp. 3925–3933, Jun. 2016.
[31] R. P. Aguilera and D. E. Quevedo, "On the stability of MPC with a finite input alphabet," *IFAC Proc. Volumes*, vol. 44, no. 1, pp. 7975–7980, 2011.
[32] M. N. Zeilinger, M. Morari, and C. N. Jones, "Soft constrained model predictive control with robust stability guarantees," *IEEE Trans. Autom. Control*, vol. 59, no. 5, pp. 1190–1202, May 2014.
[33] L. Zhang, S. Zhuang, and R. D. Braatz, "Switched model predictive control of switched linear systems: Feasibility, stability and robustness," *Automatica*, vol. 67, pp. 8–21, 2016.
[34] M. Ayala *et al.*, "Comparative study of predictive control strategies at fixed switching frequency for an asymmetrical six-phase induction motor drive," in *Proc. IEEE Int. Electric Mach. Drives Conf.*, 2017, pp. 1–8.
[35] Y. Zhao and T. Lipo, "Space vector PWM control of dual three-phase induction machine using vector space decomposition," *IEEE Trans. Ind. Electron.*, vol. 31, no. 5, pp. 1100–1109, Sep./Oct. 1995.
[36] C. Martín, M. R. Arahal, F. Barrero, and M. J. Durán, "Multiphase rotor current observers for current predictive control: A five-phase case study," *Control Eng. Pract.*, vol. 49, pp. 101–111, 2016.
[37] J. Rodas, F. Barrero, M. R. Arahal, C. Martín, and R. Gregor, "Online estimation of rotor variables in predictive current controllers: A case study using five-phase induction machines," *IEEE Trans. Ind. Electron.*, vol. 63, no. 9, pp. 5348–5356, Sep. 2016.
[38] J. Rodas, C. Martin, M. R. Arahal, F. Barrero, and R. Gregor, "Influence of covariance-based ALS methods in the performance of predictive controllers with rotor current estimation," *IEEE Trans. Ind. Electron.*, vol. 64, no. 4, pp. 2602–2607, Apr. 2017.
[39] J. Rodriguez *et al.*, "State of the art of finite control set model predictive control in power electronics," *IEEE Trans. Ind. Inform.*, vol. 9, no. 2, pp. 1003–1016, May 2013.
[40] B. Majmunović, T. Dragičević, and F. Blaabjerg, "Multi objective modulated model predictive control of stand-alone voltage source converters," *IEEE Trans. Emerg. Sel. Topics Power Electron.*, vol. 8, no. 3, pp. 2559–2571, Sep. 2020.
[41] D. Q. Mayne, J. B. Rawlings, C. V. Rao, and P. O. Scokaert, "Constrained model predictive control: Stability and optimality," *Automatica*, vol. 36, no. 6, pp. 789–814, 2000.
[42] R. P. Aguilera and D. E. Quevedo, "Stability analysis of quadratic MPC with a discrete input alphabet," *IEEE Trans. Autom. Control*, vol. 58, no. 12, pp. 3190–3196, Dec. 2013.
[43] A. G. Yepes *et al.*, "Parameter identification of multiphase induction machines with distributed windings part 1: Sinusoidal excitation methods," *IEEE Trans. Energy Conv.*, vol. 27, no. 4, pp. 1056–1066, Dec. 2012.
[44] J. A. Riveros *et al.*, "Parameter identification of multiphase induction machines with distributed windings part 2: Time-domain techniques," *IEEE Trans. Energy Convers.*, vol. 27, no. 4, pp. 1067–1077, Dec. 2012.

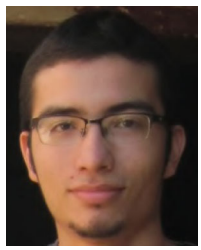

Magno Ayala received the B.Eng. degree in electronic engineering and the M.Sc. and Ph.D. degrees in power electronics from the Universidad Nacional de Asunción (UNA), San Lorenzo, Paraguay, in 2014, 2017 and 2020, respectively.

He was with the Laboratory of Power and Control System, UNA, in 2015, as a Research Assistant. His research focuses on the areas of control of multiphase ac machines.

Jesús Doval-Gandoy (Member, IEEE) received the M.Sc. degree from the Polytechnic University of Madrid, Madrid, Spain, in 1991, and the Ph.D. degree from the University of Vigo, Vigo, Spain, in 1999.

From 1991 to 1994, he was with industry. He is currently a Professor and the Head of the Applied Power Electronics Technology Research Group (APET), Universidade Vigo. His research focuses on the areas of ac power conversion.

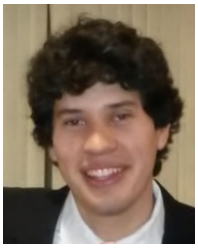

Osvaldo Gonzalez was born in Paraguay in 1987. He received the B.Eng. degree in electronic engineering and the M.Sc. degree in power electronics from the Universidad Nacional de Asunción, San Lorenzo, Paraguay, in 2014 and 2017, repsectively.

His research focuses on the area of control of multiphase motors.

Mr. Gonzalez is a recipient of the Training Program for University Lecturers from the CONACYT of Paraguay for the Ph.D. studies.

Jorge Rodas (Senior Member, IEEE) was born in Asunción, Paraguay in 1984. He received the B.Eng. degree in electronic engineering from the Universidad Nacional de Asunción, San Lorenzo, Paraguay, in 2009, the M.Sc. degrees from the Universidad de Vigo, Vigo, Spain, in 2012 and from the Universidad de Sevilla, Seville, Spain, in 2013, and the joint Ph.D. degree from the Universidad Nacional de Asunción and from the Universidad de Seville, in 2016.

In 2011, he was with the Laboratory of Power and Control Systems, Faculty of Engineering, UNA, where he is currently a Professor. His research focuses on applications of advanced control to real-world problems and his current research interests include applying model-based predictive control and nonlinear control to power electronic converters, renewable energy conversion systems, electric motor drives, and robotic systems (especially drones).

Raúl Gregor was born in Asunción, Paraguay, in 1979. He received the bachelor's degree in electronic engineering from the Catholic University of Asunción, Asunción, Paraguay, in 2005, and the M.Sc. and Ph.D. degrees in electronic, signal processing, and communications from the Higher Technical School of Engineering, University of Seville, Seville, Spain, in 2008 and 2010, respectively.

Since March 2010, he has been the Head of Engineering Faculty, Laboratory of Power and Control System, National University of Asunción, Paraguay. He has authored or coauthored about 40 technical papers in the field of power electronics and control systems, six of which have been published in high impact factor journals. His research interests include multiphase drives, advanced control of power converters topologies, quality of electrical power, renewable energy, modeling, simulation, optimization and control of power systems, smart metering and smart grids, and predictive control.

Prof. Gregor was the recipient of the Best Paper Award for the IEEE TRANSACTIONS ON INDUSTRIAL ELECTRONICS from Industrial Electronics Society, in 2010, and for the *IET Electric Power Applications*, in 2012.

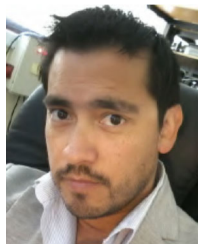

Marco Rivera (Senior Member, IEEE) was born in Talca, Chile, in 1982. He received the B.Sc. degree in electronics engineering and the M.Sc. degree in electronic engineering in electrical engineering from the Universidad de Concepción, Concepción, Chile, in 2007 and 2008, respectively, and the Ph.D. degree from the Department of Electronics Engineering, Universidad Técnica Federico Santa María, Valparaíso, Chile, in 2011.

He is currently the Head of the Laboratory of Energy Conversion and Power Electronics and the Technology Center for Energy Conversion.